

Renormalization of $(2 + 1)D$ scalar Weyl spinors interactions on lattices using the Clifford groups

Sadataka Furui

(Formerly) Graduate School of Science and Engineering, Teikyo University, Utsunomiya, 320 Japan *

(Dated: July 19, 2021)

We consider symplectic quaternions instead of unitary spinors sitting on a lattice, and calculate the fixed point Wilson action on a finite $2D$ plane expanded by $u_1ae_1 + u_2ae_2$ and on two $2D$ planes separated by $ae_1 \wedge e_2$. Only the nearest neighbor interactions are considered. Following Migdal and Kadanoff, we perform the renormalization of the Wilson action by making the lattice spacing $(\frac{1}{2})^h a$ ($h = 0, \dots, 11$), in order to simulate bosonic and solitonic phonon propagation in materials. Renormalization group method of Benfatto and Gallavotti for $(2 + 1)D$ scalar ϕ^4 system for sound propagation in Fermi sea is applied and feasibility of numerical simulation is discussed.

I. INTRODUCTION

In [1], an outline of performing a simulation of phonetic solitons propagating on $(2 + 1)D$ plane was proposed. We start from 4×4 lattices surrounded by Clifford pairs, and by adopting the renormalization group method, calculate the correlations of ultra-sonic phonetic solitons.

A main difference from standard methods is on each lattice site quaternions following symplectic groups are sitting, not spin following unitary groups.

We considered the fixed point Wilson actions in one loop adopted by deGrand et al.[2]. They considered in the $(3 + 1)D$ lattice, 28 Fixed point (FP) actions of length less than or equal to 8 lattice lengths. We classify the FP actions to *Loopc* which consist of loops on one $2D$ plane expanded by e_1 and e_2 , and *Loopd* which consist of loops on two parallel $2D$ planes connected by two links in the direction $e_1 \wedge e_2$ and in the direction $e_2 \wedge e_1$. The *Loop1, 2, 5, 6, 11, 12, 18* and *28* belong to the *LoopC* and the *Loop3, 4, 7, 8, 9, 10, 13, 14, 15, 16, 17* and *26, 27* belong to the *LoopD*. *Loop19, \dots, 25* are irrelevant in $(2 + 1)D$.

In abstract graph theory of Luescher[3] a loop in a graph is a non-empty subset of lines with the property that there exists a sequence v_1, \dots, v_N of pairwise different vertices and a labelling ℓ_1, \dots, ℓ_N of the lines in a loop, such that v_k, v_{k+1} are the end points of ℓ_k ($k = 1, \dots, N - 1$) and v_N, v_1 are end points of ℓ_N . On every loop there are two orientations, and a crossing of two loops produces a new vertex.

In this sense, the *Loop28* is not a proper loop. In [2], the loop did not play important roles, and we also observed that the eigenvalues of the action are large. We did not consider the *Loop26* and *27* which are shown in Fig.1 since eigenvalues were large, but we consider these loops in $(2 + 1)D$ space, since they are proper.



FIG. 1. Loop26 (left) and Loop27 (right).

Depending on the direction of the link between two planes, we consider paths

Loop26 α : $\mathbf{u} \rightarrow \mathbf{u} + ae_1 \rightarrow \mathbf{u} + ae_1 + ae_2 \rightarrow \mathbf{u} + ae_1 + ae_2 + ae_1 \wedge e_2 \rightarrow \mathbf{u} + ae_1 + ae_1 \wedge e_2 \rightarrow \mathbf{u} + ae_1 \rightarrow \mathbf{u} + ae_1 + ae_2 \rightarrow \mathbf{u} + ae_2 \rightarrow \mathbf{u}$, and

Loop26 β : $\mathbf{u} \rightarrow \mathbf{u} + ae_1 \rightarrow \mathbf{u} + ae_1 + ae_2 \rightarrow \mathbf{u} + ae_1 + ae_2 + ae_2 \wedge e_1 \rightarrow \mathbf{u} + ae_1 + ae_2 \wedge e_1 \rightarrow \mathbf{u} + ae_1 \rightarrow \mathbf{u} + ae_1 + ae_2 \rightarrow \mathbf{u} + ae_2 \rightarrow \mathbf{u}$.

* furui@umb.teikyo-u.ac.jp

Similarly the paths

Loop27 α : $\mathbf{u} \rightarrow \mathbf{u} + ae_1 \rightarrow \mathbf{u} + ae_1 + ae_2 \rightarrow \mathbf{u} + ae_1 + ae_2 + ae_1 \wedge e_2 \rightarrow \mathbf{u} + ae_1 + ae_1 \wedge e_2 \rightarrow \mathbf{u} + ae_1 \wedge e_2 \rightarrow \mathbf{u} + ae_2 + ae_1 \wedge e_2 \rightarrow \mathbf{u} + ae_2 \rightarrow \mathbf{u}$, and

Loop27 β : $\mathbf{u} \rightarrow \mathbf{u} + ae_1 \rightarrow \mathbf{u} + ae_1 + ae_2 \rightarrow \mathbf{u} + ae_1 + ae_2 + ae_2 \wedge e_1 \rightarrow \mathbf{u} + ae_1 + ae_2 \wedge e_1 \rightarrow \mathbf{u} + ae_2 \wedge e_1 \rightarrow \mathbf{u} + ae_2 + ae_2 \wedge e_1 \rightarrow \mathbf{u} + ae_2 \rightarrow \mathbf{u}$.

In the two loops α and β , the blue circle and the red circle are to be interchanged.

The eigenvalues of loops have dependence on the direction of paths. Difference of eigenvalues between *Loop26 α* and *Loop26 β* is larger than that of *Loop27 α* and *Loop27 β* . Their eigenvalues are about the same as those of *Loop28*.

The dependence of eigenvalues on the direction of $e_1 \wedge e_2$ shows a presence of time reversal symmetric but rotational symmetry breaking phase.

We evaluate Wilson's optimum plaquet actions by making a linear combination of eigenvalues of selected FP actions.

The structure of this presentation is as follows. In Sec. II, we compare eigenvalues $\chi(L^{(h)})$ of *LoopC* and *LoopD* for a lattice spacing a used in [16] and $a/2$. The similar analysis for the trace of link variables are given in Sec. III. In Sec. IV, a perspective of the renormalization group analysis using supercomputer are given.

II. LATTICE SPACING DEPENDENCE OF EIGENVALUES OF PLAQUETTES

We consider the case in which the spacing between the lattice $\Delta x = \frac{e_i}{4}$ which is called *LoopC* and they are $\Delta x = \frac{e_i}{8}$ which are called *LoopD*.

A. Paths on one 2D plane expanded by e_1 and e_2

The *Loop1* consists of 4 sides of a square, whose eigenvalue is the smallest among the FP actions. We characterized the path by $\mathbf{u} \rightarrow \mathbf{u} + \frac{1}{4}e_1 \rightarrow \mathbf{u} + \frac{e_1}{4} + \frac{e_2}{4} \rightarrow \mathbf{u} + \frac{e_2}{4} \rightarrow \mathbf{u}$ where \mathbf{u} are mesh points $(u_1e_1 + u_2e_2)$, $0 \leq u_1, u_2 \leq 3$ ($u_i \in \mathbf{Z}$). We call the path *Loop1c*.

We compare eigenvalues of the path of $\mathbf{u} \rightarrow \mathbf{u} + \frac{1}{8}e_1 \rightarrow \mathbf{u} + \frac{e_1}{8} + \frac{e_2}{8} \rightarrow \mathbf{u} + \frac{e_2}{8} \rightarrow \mathbf{u} - \frac{1}{8}e_2 \rightarrow \mathbf{u}$, which we call *Loop1d*.

In the left figure of Fig.2, eigenvalues of $u_1 = 0$ (*blue*), 1 (*orange*), 2 (*green*), 3 (*red*) as a function of u_2 are plotted, and in the right figure of Fig.2, eigenvalues of $u_1 = 0, \frac{1}{2}, 1, \frac{3}{2}, 2, \frac{5}{2}, 3$ as a function of u_2 are plotted. When the lattice spacing is smaller, eigenvalues are smaller.

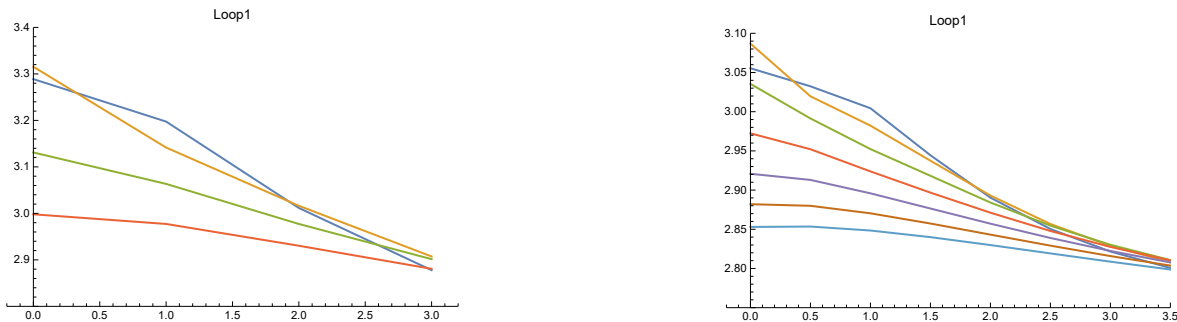


FIG. 2. Absolute values of eigenvalues for fixed u_1 in *Loop1c*(left) and in *Loop1d* (right).

The eigenvalues of *Loop28* are shown in Fig.3. The loop is not proper in the sense of Luescher[3]. Fluctuations are large for small \mathbf{u} or in infrared regions.

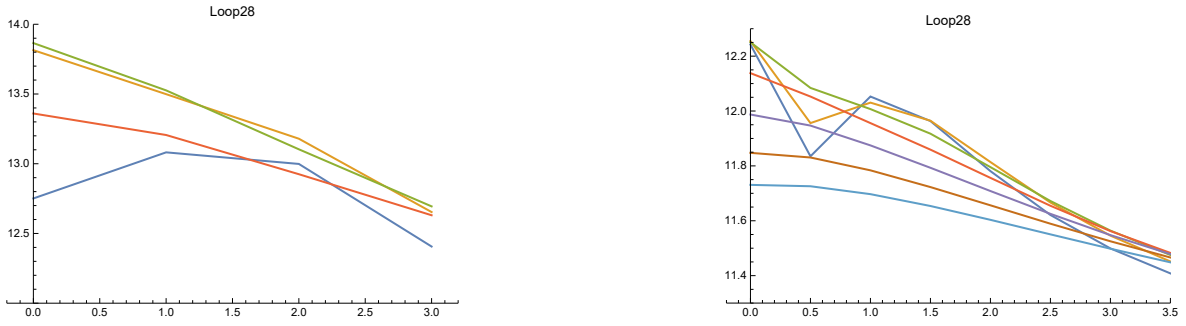


FIG. 3. Absolute values of eigenvalues for fixed u_1 in Loop28c(left) and in Loop28d(right).

The eigenvalues of *Loop2* are shown in Fig.4. Eigenvalues of the smaller lattice spacing *Loop2d* is smaller than those of *Loops2c*.

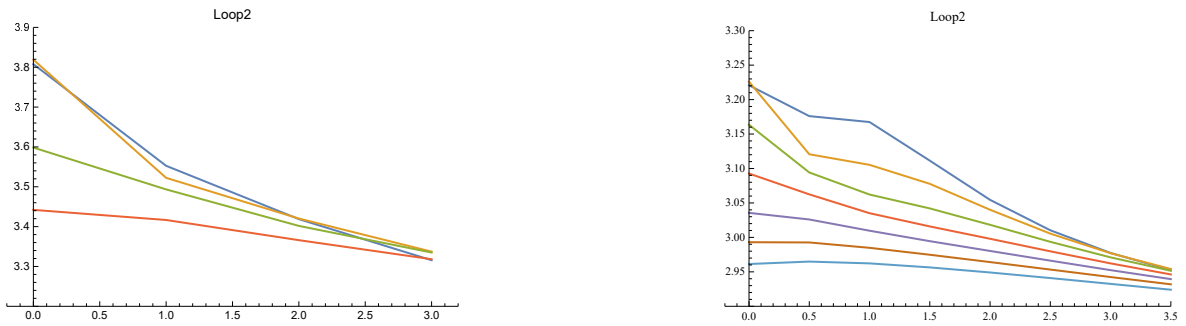


FIG. 4. Absolute values of eigenvalues for a fixed u_1 in Loop2c(left) and in Loop2d(right)

The eigenvalues of *Loop5* are shown in Fig.5. The *Loop5* has a bending point of the path at the center of the loop. It produces a large eigenvalues for small u_1 .

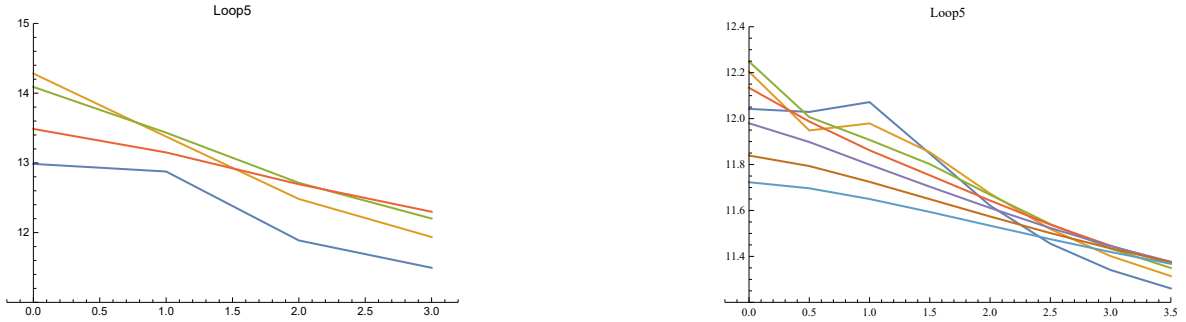


FIG. 5. Absolute values of eigenvalues for a fixed u_1 in Loop5c(left) and in Loop5d(right) .

The eigenvalues of *Loop6* are shown in Fig.6.They have \mathbf{u} dependence in the infrared region.

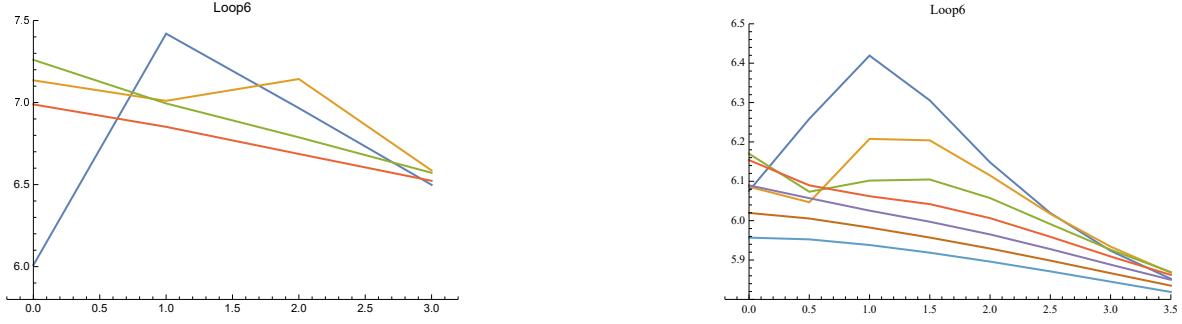


FIG. 6. Absolute values of eigenvalues for a fixed u_1 in Loop6c (left) and in Loop6d (right).

The eigenvalues of *Loop11* are shown in Fig.7.The *Loop11* has a bending due to presence of overlapping links in the center.

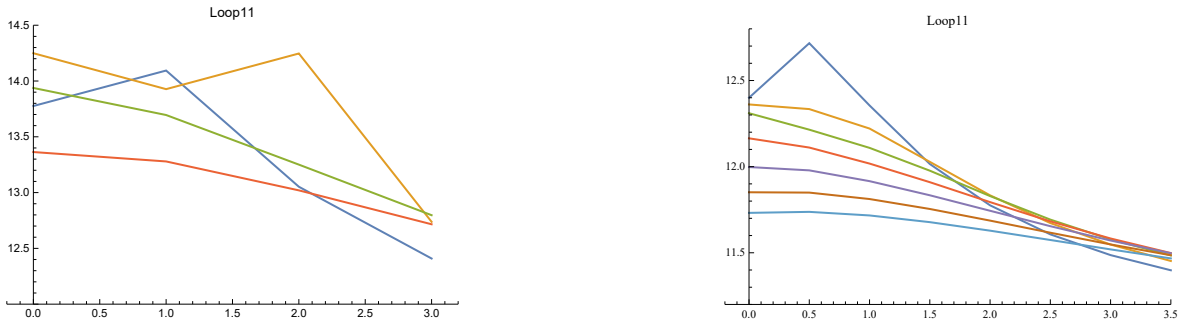


FIG. 7. Absolute values of eigenvalues for a fixed u_1 in Loop11c (left) and in Loop11d (right).

The eigenvalues of *Loop12* are shown in Fig.8, The *Loop12* is similar to the *Loop5*, but there is a self-crossing of two long links at the center. The \mathbf{u} dependence of eigenvalues of *Loop5* and *Loop12* are similar, but absolute values of eigenvalues of *Loop12* are smaller, due to presence of long links. In the $(3+1)D$ lattice simulation of [2], the *Loop5* is more effective than *Loop12*.

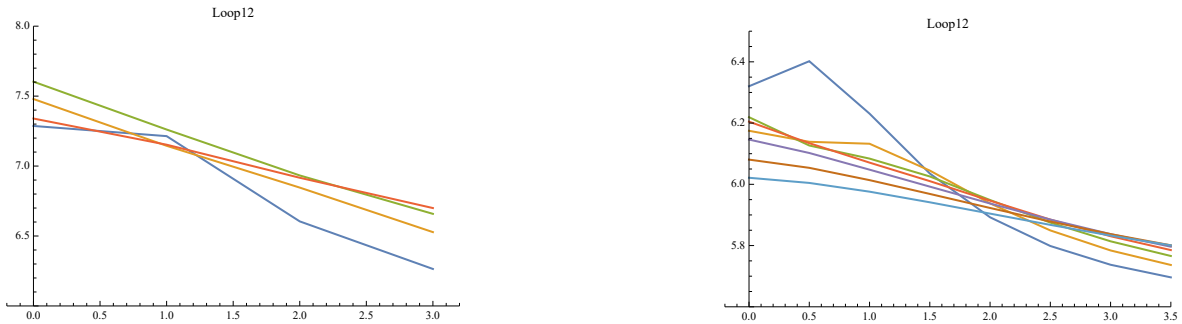


FIG. 8. Absolute values of eigenvalues for a fixed u_1 in Loop12c (left) and in Loop12d(right). .

In [1], the starting point of the *Loop18* was chosen to be same as the *Loop1*, and only the scale was changed. In this paper we replace the verices as those of the paper [2],

$$L18[u_1, u_2] = t1[-\frac{1}{4}, u_1 + \frac{1}{4}, u_2] \times t2[-\frac{1}{2}, u_1 + \frac{1}{4}, u_2 + \frac{1}{2}] \times t1[-\frac{1}{2}, u_1 + \frac{1}{4}, u_2 + \frac{1}{2}] \times t2[\frac{1}{2}, u_1 + \frac{1}{4}, u_2] \times t1[\frac{1}{4}, u_1, u_2].$$

The eigenvalues of the new *Loop18* and its lattice scalings halved are shown in Fig.9.The *Loop18* contains long straight links parallel to e_2 .

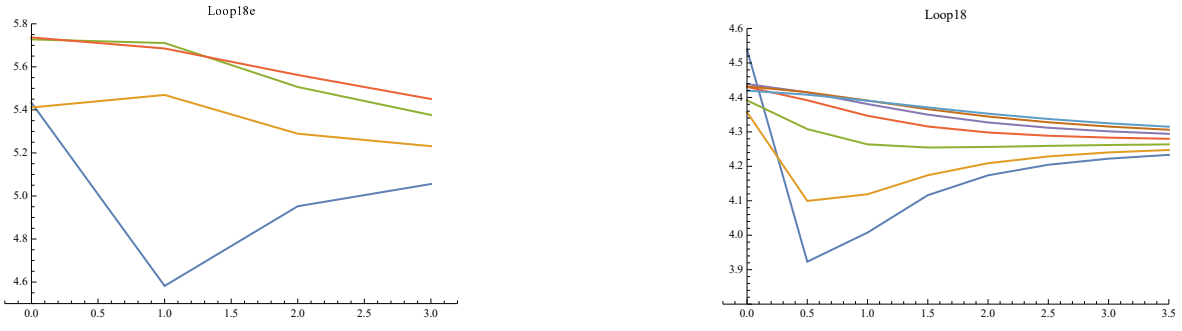


FIG. 9. Absolute values of eigenvalues for a fixed u_1 in Loop18c (left) and in Loop18d (right).

B. Paths on two planes connected by $e_1 \wedge e_2$

When there are links between two $2D$ planes, a problem of choice of scale of length between the two $2D$ planes appears. We leave it as a future study, and calculate eigenvalues using the same lattice spacing between the $2D$ planes and on the $2D$ plane.

The paths on two planes we considered in [16] were restricted to α type. Since eigenvalues in the large \mathbf{u} region are almost independent of α and β , we restrict loops to be α type and consider β type near the final stage of MonteCarlo simulation.

The path of *Loop3c* consists of $\mathbf{u} \rightarrow \mathbf{u} + \frac{1}{4}e_1 \rightarrow \mathbf{u} + \frac{1}{4}e_1 + \frac{1}{4}e_2 \rightarrow \mathbf{u} + \frac{1}{4}e_1 + \frac{1}{4}e_2 + \frac{1}{4}e_1 \wedge e_2 \rightarrow \mathbf{u} + \frac{1}{4}e_1 + \frac{1}{4}e_1 \wedge e_2 \rightarrow \mathbf{u} + \frac{1}{4}e_1 \wedge e_2 \rightarrow \mathbf{u}$.

The path of *Loop3d* consists of $\mathbf{u} \rightarrow \mathbf{u} + \frac{1}{8}e_1 \rightarrow \mathbf{u} + \frac{1}{8}e_1 + \frac{1}{8}e_2 \rightarrow \mathbf{u} + \frac{1}{8}e_1 + \frac{1}{8}e_2 + \frac{1}{8}e_1 \wedge e_2 \rightarrow \mathbf{u} + \frac{1}{8}e_1 + \frac{1}{8}e_1 \wedge e_2 \rightarrow \mathbf{u} + \frac{1}{8}e_1 \wedge e_2 \rightarrow \mathbf{u}$.

The eigenvalues of *Loop3* are shown in Fig.10. We observe the eigenvalues of action of *Loop3* is roughly about twice of those of *Loop1*.

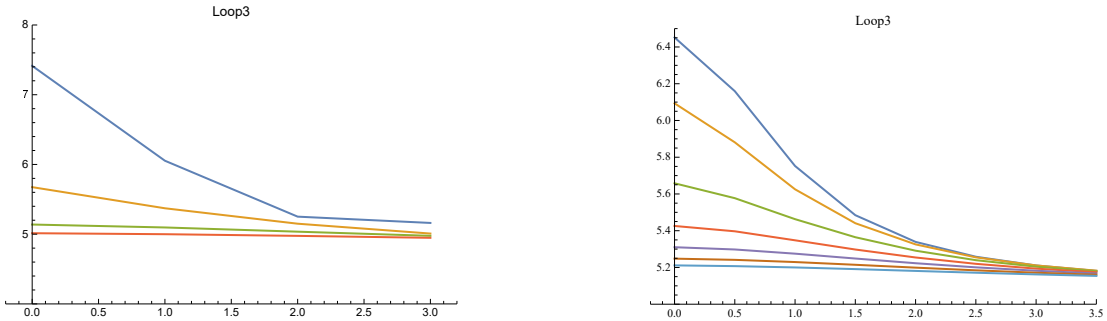


FIG. 10. Absolute values of eigenvalues for a fixed u_1 in Loop3c (left) and in Loop3d(right).

The eigenvalues of *Loop4* are shown in Fig.11.

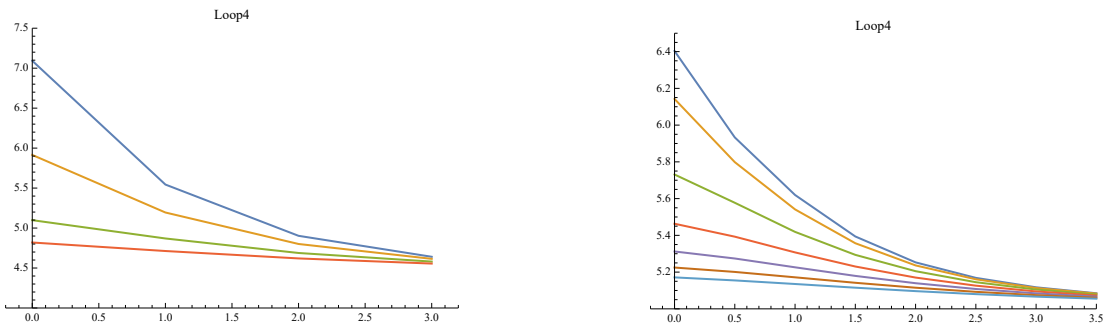


FIG. 11. Absolute values of eigenvalues for a fixed u_1 in Loop4c (left) and in Loop4d(right).

The eigenvalues of *Loop7* are shown in Fig.12.

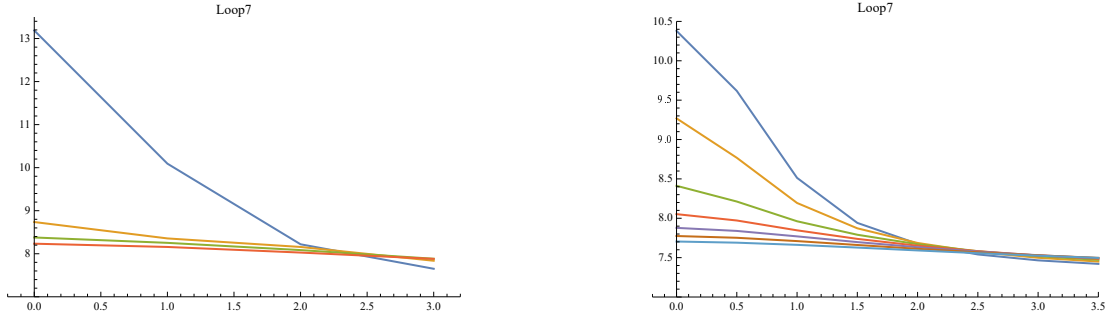


FIG. 12. Absolute values of eigenvalues for a fixed u_1 in Loop7c (left) and in Loop7d (right).

The eigenvalues of *Loop8* are shown in Fig.13.

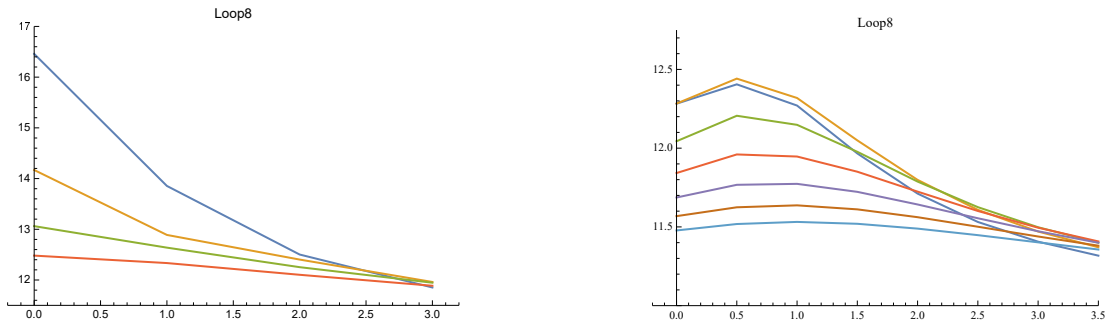


FIG. 13. Absolute values of eigenvalues for a fixed u_1 in Loop6c (left) and in Loop8d(right).

The eigenvalues of *Loop9* are shown in Fig.14 .

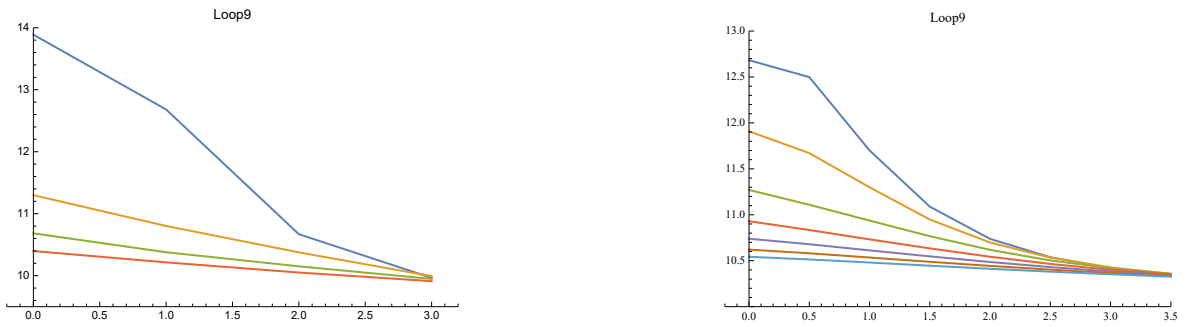


FIG. 14. Absolute values of eigenvalues for a fixed u_1 in Loop9c(left) and in Loop9d(right).

The eigenvalues of *Loop10* are shown in Fig.15.

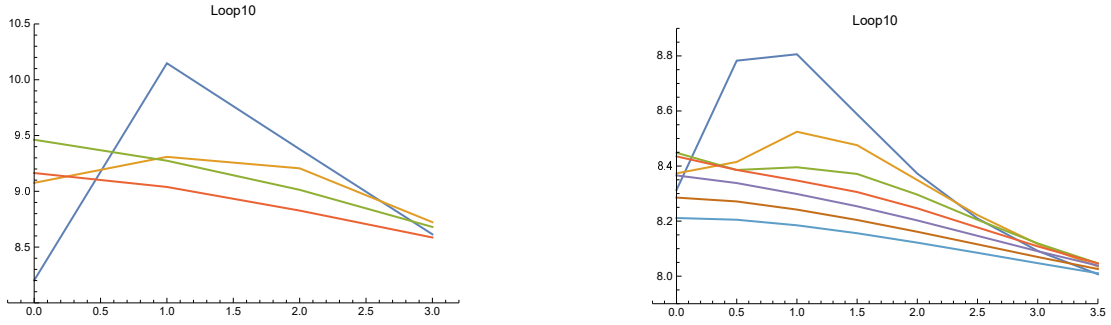


FIG. 15. Absolute values of eigenvalues for a fixed u_1 in Loop10c(left) and in Loop10d(right).

The eigenvalues of *Loop13* are shown in Fig.16.

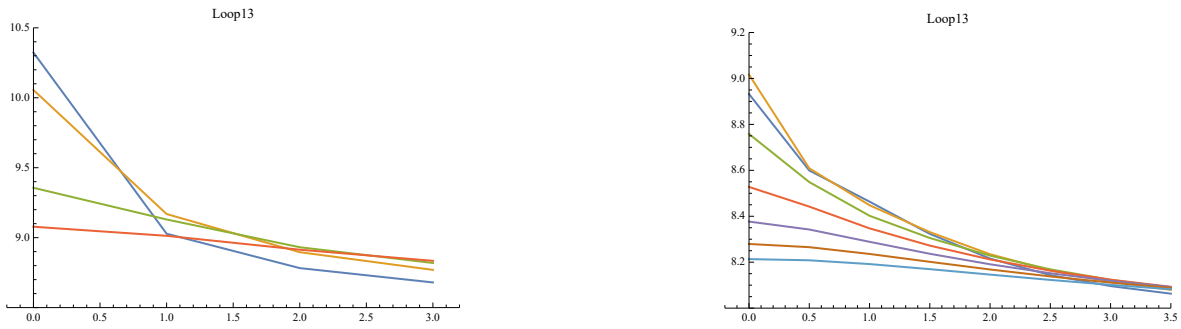


FIG. 16. Absolute values of eigenvalues for a fixed u_1 in Loop13c (left) and in Loop13d(right).

The eigenvalues of *Loop14* are shown in Fig.17 .

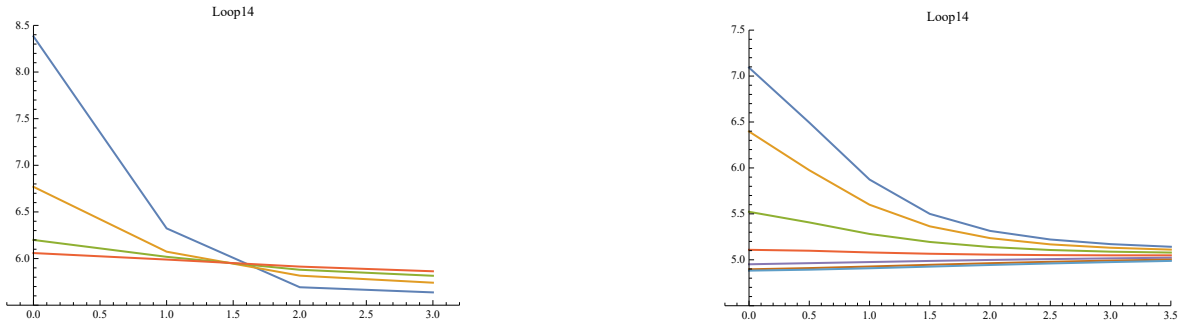


FIG. 17. Absolute values of eigenvalues for a fixed u_1 in Loop14c (left) and in Loop14d(right).

The eigenvalues of *Loop15* are shown in Fig.18. The eigenvalues of *Loop16* are shown in Fig.19 .

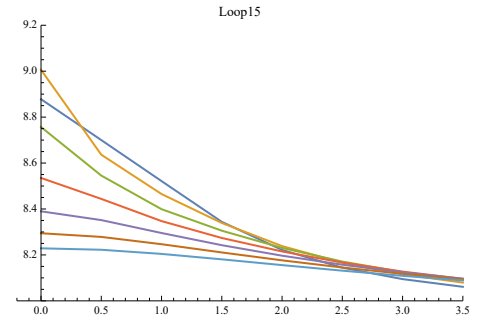
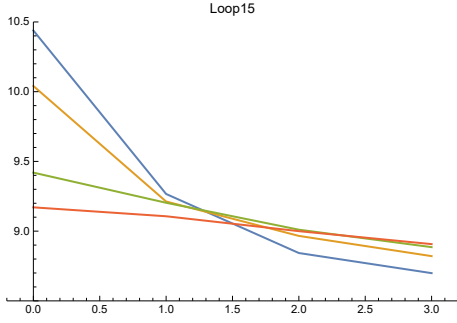


FIG. 18. Absolute values of eigenvalues for a fixed u_1 in Loop15c(left) and in Loop15d (right).

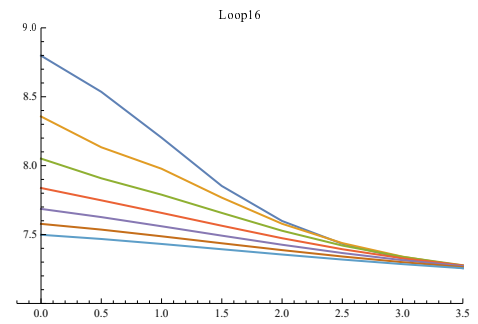
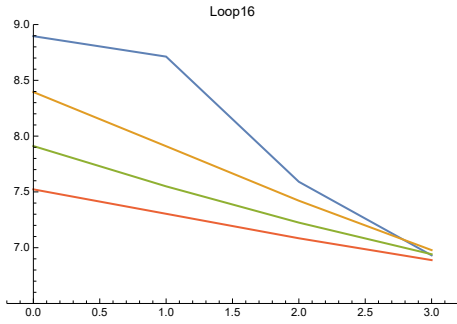


FIG. 19. Absolute values of eigenvalues for a fixed u_1 in Loop16c(left) and in Loop16d(right).

The eigenvalues of *Loop17* are shown in Fig.20.

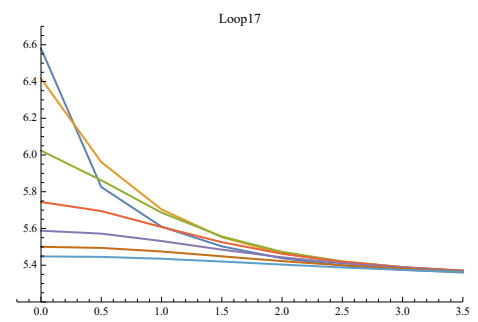
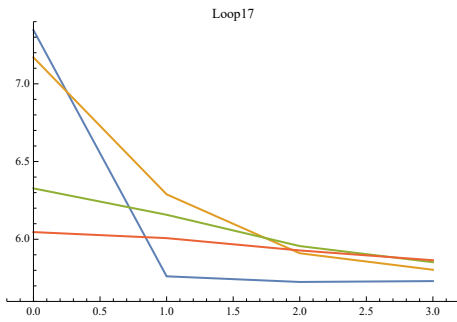


FIG. 20. Absolute values of eigenvalues for a fixed u_1 in Loop17c (left) and in Loop17d(right).

The eigenvalues of the $Loop26\alpha$ and $Loop26\beta$ of $a = 1/8$ are shown in Fig.21

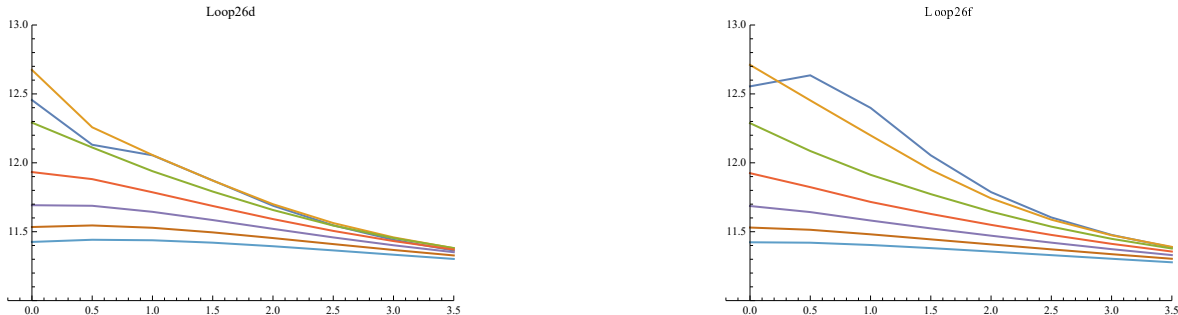


FIG. 21. Absolute values of eigenvalues for a fixed u_1 in $Loop26\alpha$ (left) and in $Loop26\beta$ (right).

The eigenvalues of the $Loop27\alpha$ and $Loop27\beta$ are shown in Fig.22

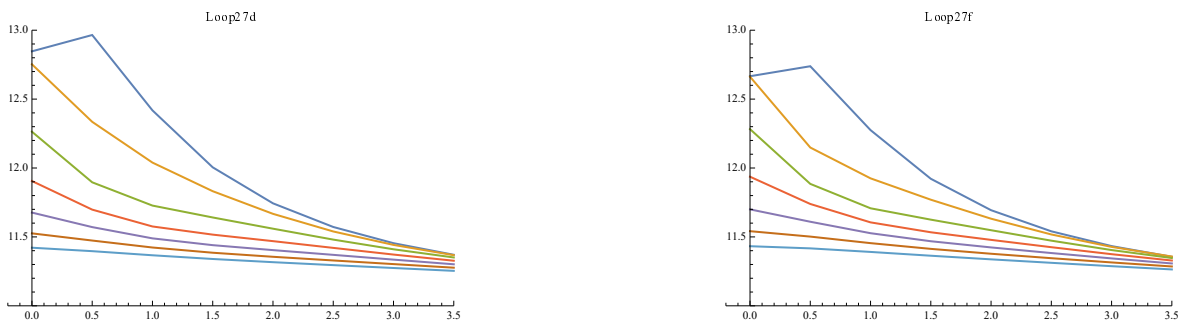


FIG. 22. Absolute values of eigenvalues for a fixed u_1 in $Loop27d$ (left) and in $Loop27f$ (right).

III. LATTICE SPACING DEPENDENCE OF TRACES OF LINK VARIABLES

In Clifford algebra, transformation of a coordinate X is represented by[13]

$$\begin{pmatrix} a & c \\ b & d \end{pmatrix} \begin{pmatrix} x & xx^- \\ 1 & x^- \end{pmatrix} \begin{pmatrix} d^- & c^- \\ b^- & a^- \end{pmatrix} = \lambda \begin{pmatrix} x' & x'x'^- \\ 1 & x'^- \end{pmatrix}$$

and the term xx^- yields link products.

In lattice simulations of scalar fields, we consider Feynman path integrals is $Z = \int [d\psi] e^{-S}$ with $\mathbf{x} = a(u_1 e_1 + u_2 e_2) + au_3 e_1 \wedge e_2$, $-N/2 < u_1, u_2, u_3 \leq N/2$, $\mu = 1, 2, 3$. $N \sim 2^{11} = 2048$. The scale of $e_1 \wedge e_2$ is chosen to be the same as e_1, e_2 , for Wilson loops, but it can be complex for Polyakov loops.

The expectation values of Wilson or Polyakov action S consists of eigenvalues of left lower components of the Loop matrices $Lk[u_1, u_2]$ where k specifies the FP actions of [2], and the trace of $DS(Lk[u_1, u_2])$ which consists of the sum of dS_1 and dS_2 along the loops

The 4×4 matrix of the $Loop1$ contribution

$$DS(L1[u_1, u_2]) = dS_1[u_1, u_2] + dS_2[u_1 + a, u_2] - dS_1[u_1 + a, u_2 + a] - dS_2[u_1, u_2 + a]$$

has non-zero components in the right upper component. We measure the trace of the 2×2 matrices.

In the case of $Loop2$,

$$DS(L2[u_1, u_2]) = dS_1[u_1, u_2] + 2dS_2[u_1 + a, u_2] - dS_1[u_1 + a, u_2 + 2a] - 2dS_2[u_1, u_2 + 2a]$$

has non-zero components only in the right upper corner.

A. Paths on one 2D plane expanded by e_1 and e_2

The traces of the 2×2 matrix, which is twice the real part of the diagonal component in the case of *Loop1* as a function of u_2 for fixed u_1 are shown in Fig.23.

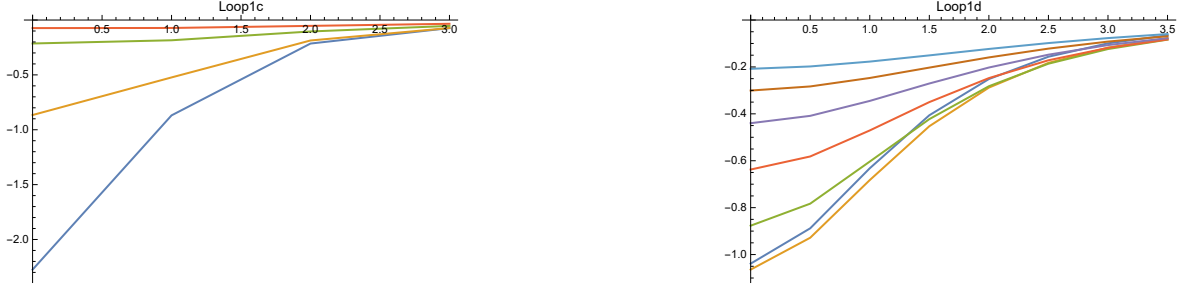


FIG. 23. Trace of $d\mathbf{S}(L1[u_1, u_2])$ for $\Delta u_i = 1$ (left) and $\Delta u_i = \frac{1}{2}$ (right). ($i = 1, 2$)

The traces of the matrix in the case of *Loop2* are shown in Fig.24.



FIG. 24. Trace of $d\mathbf{S}(L2[u_1, u_2])$ for $\Delta u_i = 1$ (left) and $\Delta u_i = \frac{1}{2}$ (right). ($i = 1, 2$)

The traces of the matrix in the case of *Loop5* are shown in Fig.25.



FIG. 25. Trace of $d\mathbf{S}(L5[u_1, u_2])$ for $\Delta u_i = 1$ (left) and $\Delta u_i = \frac{1}{2}$ (right). ($i = 1, 2$)

The traces of the matrix in the case of *Loop5* are shown in Fig.26.

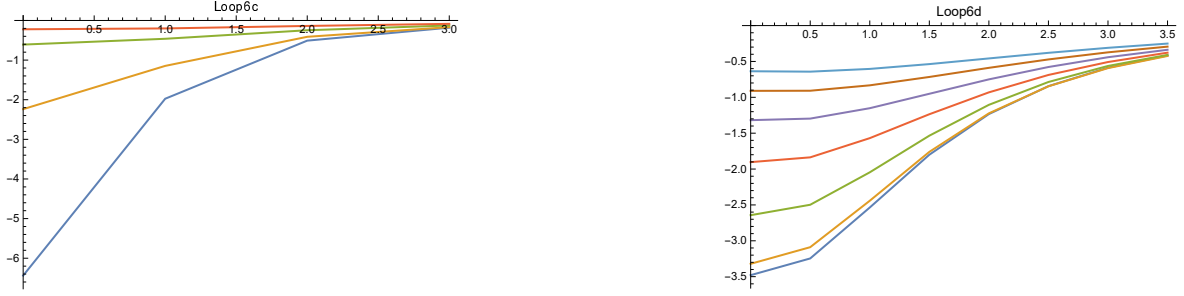


FIG. 26. Trace of $d\mathbf{S}(L6[u_1, u_2])$ for $\Delta u_i = 1$ (left) and $\Delta u_i = \frac{1}{2}$ (right). ($i = 1, 2$)

The traces of the matrix in the case of *Loop11* are shown in Fig.27.

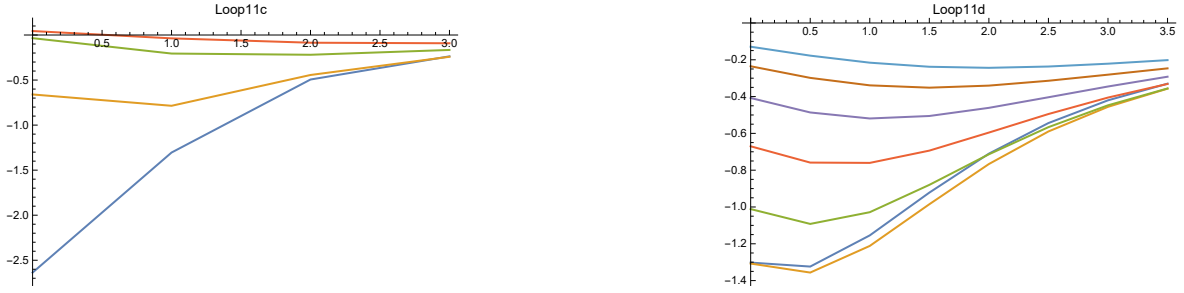


FIG. 27. Trace of $d\mathbf{S}(L11[u_1, u_2])$ for $\Delta u_i = 1$ (left) and $\Delta u_i = \frac{1}{2}$ (right). ($i = 1, 2$)

The traces of the matrix in the case of *Loop12* are shown in Fig.28.

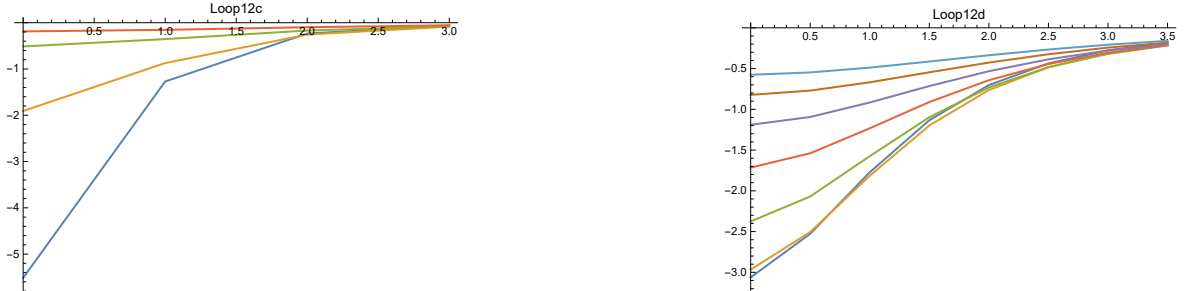


FIG. 28. Trace of $d\mathbf{S}(L12[u_1, u_2])$ for $\Delta u_i = 1$ (left) and $\Delta u_i = \frac{1}{2}$ (right). ($i = 1, 2$)

The traces of the matrix in the case of *Loop18* are shown in Fig.29..

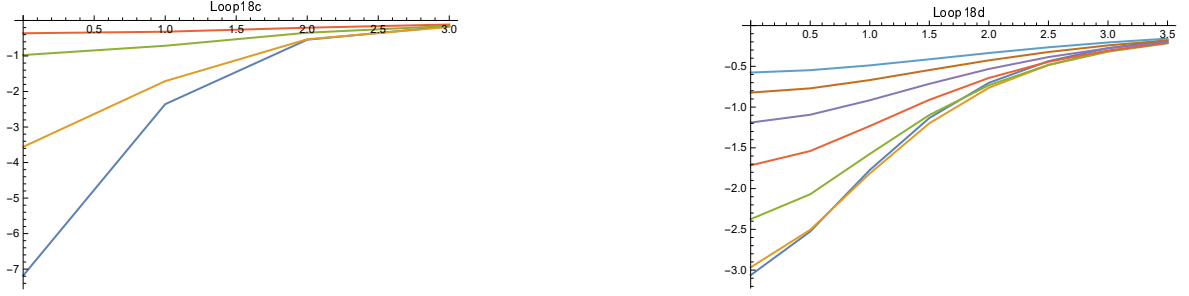


FIG. 29. Trace of $d\mathbf{S}(L18[u_1, u_2])$ for $\Delta u_i = 1$ (left) and $\Delta u_i = \frac{1}{2}$ (right). ($i = 1, 2$)

B. Paths on two planes connected by $e_1 \wedge e_2$

The traces of the matrix in the case of *Loop3* are shown in Fig.30.



FIG. 30. Trace of $d\mathbf{S}(L3[u_1, u_2])$ for $\Delta u_i = 1$ (left) and $\Delta u_i = \frac{1}{2}$ (right). ($i = 1, 2$)

The traces of the matrix in the case of *Loop4* are shown in Fig.31.



FIG. 31. Trace of $d\mathbf{S}(L4[u_1, u_2])$ for $\Delta u_i = 1$ (left) and $\Delta u_i = \frac{1}{2}$ (right). ($i = 1, 2$)

The traces of the matrix in the case of *Loop7* are shown in Fig.32.

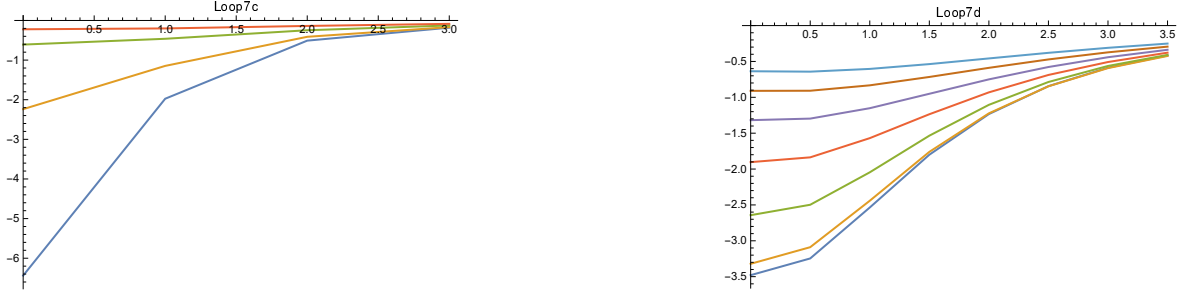


FIG. 32. Trace of $d\mathbf{S}(L7[u_1, u_2])$ for $\Delta u_i = 1$ (left) and $\Delta u_i = \frac{1}{2}$ (right). ($i = 1, 2$)

The traces of the matrix in the case of *Loop8* are shown in Fig.33.



FIG. 33. Trace of $d\mathbf{S}(L8[u_1, u_2])$ for $\Delta u_i = 1$ (left) and $\Delta u_i = \frac{1}{2}$ (right.) ($i = 1, 2$)

The traces of the matrix in the case of *Loop9* are shown in Fig.34.



FIG. 34. Trace of $d\mathbf{S}(L9[u_1, u_2])$ for $\Delta u_i = 1$ (left) and $\Delta u_i = \frac{1}{2}$ (right). ($i = 1, 2$)

The traces of the matrix in the case of *Loop10* are shown in Fig.35.

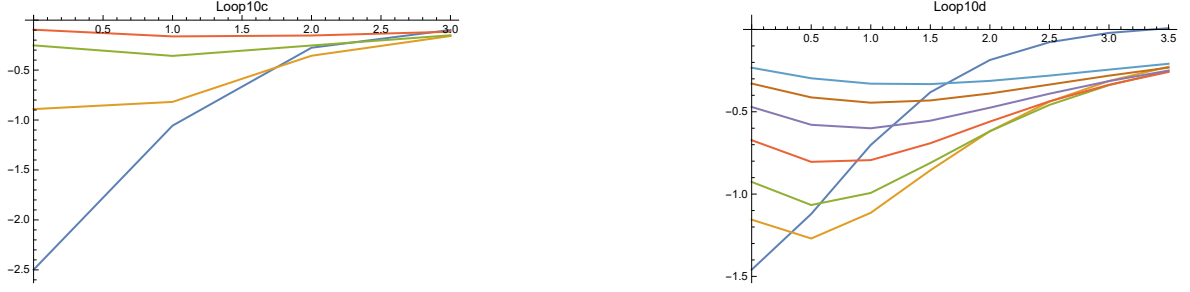


FIG. 35. Trace of $d\mathbf{S}(L10[u_1, u_2])$ for $\Delta u_i = 1$ (left) and $\Delta u_i = \frac{1}{2}$ (right). ($i = 1, 2$)

The traces of the matrix in the case of *Loop13* are shown in Fig.36.



FIG. 36. Trace of $d\mathbf{S}(L13[u_1, u_2])$ for $\Delta u_i = 1$ (left) and $\Delta u_i = \frac{1}{2}$ (right). ($i = 1, 2$)

The traces of the matrix in the case of *Loop14* are shown in Fig.37.



FIG. 37. Trace of $d\mathbf{S}(L14[u_1, u_2])$ for $\Delta u_i = 1$ (left) and $\Delta u_i = \frac{1}{2}$ (right). ($i = 1, 2$)

The traces of the matrix in the case of *Loop15* are shown in Fig.38.

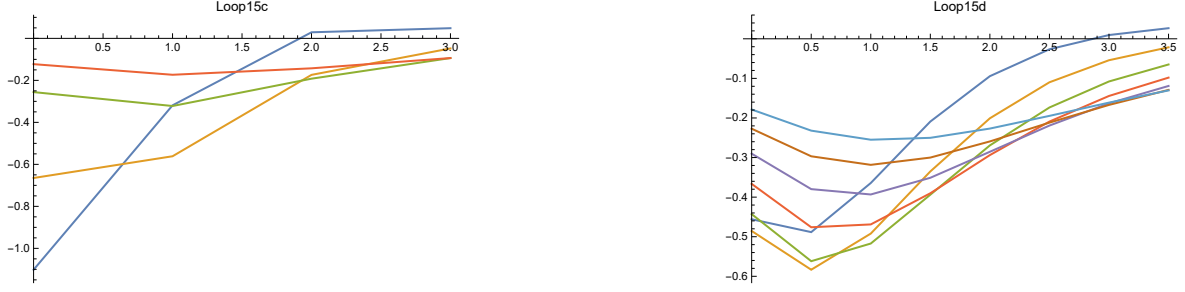


FIG. 38. Trace of $d\mathbf{S}(L15[u_1, u_2])$ for $\Delta u_i = 1$ (left) and $\Delta u_i = \frac{1}{2}$ (right). ($i = 1, 2$)

The traces of the matrix in the case of *Loop16* are shown in Fig.39.

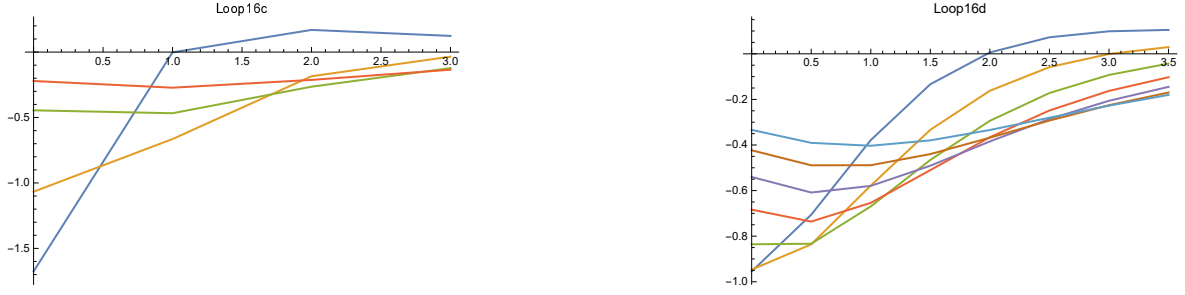


FIG. 39. Trace of $d\mathbf{S}(L16[u_1, u_2])$ for $\Delta u_i = 1$ (left) and $\Delta u_i = \frac{1}{2}$ (right). ($i = 1, 2$)

The traces of the matrix in the case of *Loop17* are shown in Fig.40.

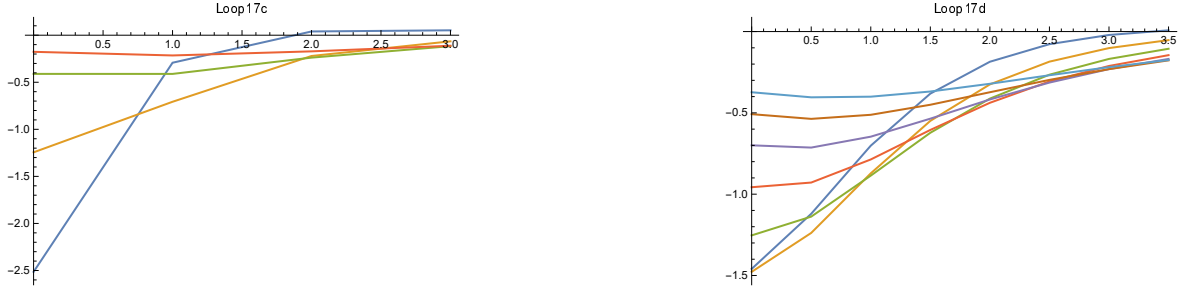


FIG. 40. Trace of $d\mathbf{S}(L17[u_1, u_2])$ for $\Delta u_i = 1$ (left) and $\Delta u_i = \frac{1}{2}$ (right). ($i = 1, 2$)

The traces of the matrix in the case of *Loop26* are shown in Fig.41.



FIG. 41. Trace of $d\mathbf{S}(L26[u_1, u_2])$ for $\Delta u_i = 1$ (left) and $\Delta u_i = \frac{1}{2}$ (right). ($i = 1, 2$)

The traces of the matrix in the case of *Loop27* are shown in Fig.42.



FIG. 42. Trace of $d\mathbf{S}(L27[u_1, u_2])$ for $\Delta u_i = 1$ (left) and $\Delta u_i = \frac{1}{2}$ (right). ($i = 1, 2$)

IV. DISCUSSION AND PERSPECTIVE

We expected that correlation of phonons and its time-reversed phonons propagating on a $2D$ plane can be simulated by a model of Bosonic quasiparticle propagating in the Fermionic sea of Weyl spinors.

In an exploratory analysis using Clifford algebra, we observed that as the lattice spacing a is halved, eigenvalues of the FP Wilson action and the trace of the matrix representing links of Loops surrounding each FP Wilson action are reduced. Monte-Carlo simulations using a small lattice constant a will allow fixing the optimal Wilson action or the Polyakov action as a linear combination of the FP actions with correction terms derived by the renormalization group.

There are works on the study of Quantum spin systems associated with time translations and space translations of lattice spaces[14, 15]. Solitons are integrable systems induced by nonlinear interactions. Detailed comparison between experiments and simulation will clarify the Kubo-Martin-Schwinger boundary condition.

We have a plan of reducing a and perform the renormalization group analysis using supercomputers which allow parallel computations. Whether one can connects the chiral anomaly and gravitation anomaly by simulating the ultrasonic waves remains as a future study.

ACKNOWLEDGMENTS

I thank Dr. Serge DosSantos at INSA for valuable discussion and Prof. M. Arai for supports. Thanks are also due to the CMC of Osaka University for allowing use of super computers there, which were developed by CMC and Tokyo Institute of Technology.

-
- [1] Sadataka Furui, *Lattice simulation of (2+1)D phonetic solitons and the Renormalization group*, arXiv: 2105.06265[hep-lat].
 - [2] T.DeGrand, A. Hasenfratz, P. Hasenfratz, and F. Niedermayer, *Non-perturbative tests of the fixed point action for SU(3) gauge theory*, Nucl. Phys. **B 454**, 615-637 (1995); arXiv: hep-lat/9506031 (1995).
 - [3] M. Luescher, *Volume Dependence of the Energy Spectrum in Massive Quantum Field Theories*, I. Stable Particle States, Commun. Math. Phys. **104**, 177-206 (1986).
 - [4] Michael Creutz, *Quarks, gluons and lattices*, Cambridge Monographs on Mathematical Physics, Cambridge (1983).
 - [5] P. Hasenfratz and F. Niedermayer, *Fixed-Point Actions in 1-Loop Perturbation Theory*, arXiv:hep-lat/9706002 v1 (1997).
 - [6] K.G. Wilson, *Renormalization Group and Critical Phenomena, I. Renormalization Group and the Kadanoff Scaling Picture*, Phys. Rev. **B4**(9) 3174-3183 (1971).
 - [7] K.G. Wilson, *Renormalization Group and Critical Phenomena, II. Phase-Space Cell Analysis of Critical Behavior*, Phys. Rev. **B4**(9) 3184-3205 (1971).
 - [8] Kenneth G. Wilson, *Confinement of quarks*, Phys. Rev. **D 10**(8) 2445-2459 (1974).
 - [9] Giovanni Gallavotti, *Renormalization theory and ultraviolet stability for scalar fields via renormalization group methods*, Rev. Mod. Phys. **57**, 471-562 (1985).
 - [10] G. Benfatto and G. Gallavotti, *Renormalization-group approach to the theory of the Fermi surface*, Phys. Rev. **B 42**(16) 9967-9972 (1990).
 - [11] G. Benfatto, G. Gallavotti and V. Mastropietro, *Renormalization group and the Fermi surface in the Luttinger model*, Phys. Rev. **B 45**(10) 5468-5480 (1992).
 - [12] G. Benfatto and G. Gallavotti, *Renormalization Group*, Physics Notes, Princeton University Press, Princeton New Jersey (1995).
 - [13] I.R. Porteous, *Clifford Algebras and the Classical Groups*, Cambridge studies in advanced mathematics, Cambridge (1995).
 - [14] Derek W. Robinson, *Statistical Mechanics of Quantum Spin Systems. II*, Commun. Math. Phys. **7**, 337-348 (1968).
 - [15] Elliott H Lieb and Derek W. Robinson, *The Finite Group Velocity of Quantum Spin Systems*, Commun. Math. Phys. **28**, 251-257 (1972).
 - [16] Sadataka Furui, *Supersymmetry in Hadron Spectroscopy and Solitons in 2 Dimensional Fermionic Media*, arXiv:[hep-th] 2011.03527 (v1) (2020).

Loop2c

